Int J Cardiovasc Imaging (2014) 30:857–865
DOI 10.1007/s10554-014-0422-z

ORIGINAL PAPER

Impact of strut–vessel distance and underlying plaque type on the resolution of acute strut malapposition: serial optimal coherence tomography analysis after everolimus-eluting stent implantation

Takumi Inoue · Toshiro Shinke · Hiromasa Otake · Masayuki Nakagawa · Hirotoshi Hariki · Tsuyoshi Osue · Masamichi Iwasaki · Yu Taniguchi · Ryo Nishio · Noritoshi Hiranuma · Akihide Konishi · Hiroto Kinutani · Masaru Kuroda · Ken-ichi Hirata

Received: 11 October 2013 / Accepted: 8 April 2014 / Published online: 19 April 2014

Abstract The consequences of acute strut malapposition in everolimus-eluting stents (EES) are unknown. This study investigated the impact of strut–vessel (S–V) distance and plaque type underneath acute strut malapposition on the mid-term vessel response in EES. Twenty-nine patients (35 EES) underwent optical coherence tomography (OCT) immediately after percutaneous coronary intervention and at 8-month follow-up. S–V distance and plaque type (lipid, calcified, or fibrous) underneath acute strut malapposition were evaluated. Follow-up OCT classified acute strut malapposition as persistent or resolved. The S–V cutoff value for predicting resolved strut malapposition and the incidence of intra-stent thrombi were determined. Among 569 cases of acute strut malapposition, involving 29,168 struts, 139 (24.4 %) were persistent. Mean S–V distance was significantly longer in persistent than in resolved strut malapposition (600 ± 294 vs. 231 ± 95 μm; $P < 0.0001$). S–V distance ≤380 μm was the best cutoff value for predicting resolved strut malapposition (sensitivity 93.5 %, specificity 69.8 %, area under curve 0.878). Acute strut malapposition with S–V distance ≤380 μm remained persistent more frequently over lipid/calcified than over fibrous plaques (lipid: 13.4 %, calcified: 18.2 %, fibrous: 4.2 %; lipid vs. fibrous, $P = 0.001$; calcified vs. fibrous, $P = 0.02$). Intra-stent thrombi were more frequent in stents with ≥1 persistent strut malapposition than in those without [4/11 stents (36.3 %) vs. 0/24 (0 %); $P = 0.006$]. Lipid and calcified plaque, together with S–V distance, affect the resolution of acute strut malapposition in EES. Persistent strut malapposition is associated with the presence of thrombi at follow-up, which could be the substrate for late stent thrombosis.

Keywords Optical coherence tomography · Everolimus-eluting stents · Strut malapposition · Lipid plaque

T. Inoue · T. Shinke (✉) · H. Otake · M. Nakagawa · H. Hariki · T. Osue · M. Iwasaki · Y. Taniguchi · R. Nishio · N. Hiranuma · A. Konishi · H. Kinutani · M. Kuroda · K. Hirata
Division of Cardiovascular Medicine, Department of Internal Medicine, Kobe University Graduate School of Medicine, 7-5-1 Kusunoki-cho, Chuo-ku, Kobe, Hyogo 650-0017, Japan
e-mail: shinke@med.kobe-u.ac.jp

Introduction

Monitoring of stent placement by optical coherence tomography (OCT) immediately after stent implantation in the clinical setting has enabled the visualization of various types of vessel reaction (stent malapposition, thrombus, edge dissection, and prolapse) that are too subtle to be detected by intravascular ultrasound (IVUS) [1–3]. We have demonstrated using OCT analyses that the strut–vessel wall (S–V) distance of acute strut malapposition after the implantation of first-generation drug-eluting stents (DES) might predict its persistence [4]. Recently, Gutierrez-Chico et al. [5] reported that the maximum strut malapposition distance per strut was a good predictor of persistence in 2nd generation DES, although their study had the limitations of including various stent types and follow-up durations. The impact of S–V distance on the vessel reaction to acute strut malapposition in everolimus-eluting stents (EES) is still unknown.

Aside from S–V distance, it has been hypothesized that the nature of the underlying plaque may affect the process of strut coverage, and a recent OCT study has demonstrated

a higher frequency of uncovered struts in 1st generation DES implanted for ST-elevation myocardial infarction than in those used to treat stable angina [6]. However, the impact of the underlying plaque type on the course of acute strut malapposition in EES has not been addressed.

The aim of this study was to investigate the impact of S–V distance and underlying plaque type on the natural history of acute strut malapposition in EES.

Methods

Study population and methods

Among patients who had de novo lesions in a native coronary artery and were treated with EES (Xience V, Abbott Vascular, Inc., Santa Clara, CA, USA, or Promus, Boston Scientific Corp., Natick, MA, USA) between July 2010 and November 2011, we investigated those who had undergone frequency-domain OCT (FD-OCT) analysis immediately following percutaneous coronary intervention (PCI) and 8 months after stent implantation. Target lesions fulfilled the following inclusion criteria: de novo native coronary artery lesions with $\geq$75 % diameter stenosis, reference vessel diameter 2.5–3.5 mm by visual estimation, or chronic total occlusion. Exclusion criteria were as follows: (1) acute myocardial infarction, (2) apparent congestive heart failure, (3) contraindication for dual antiplatelet therapy, and (4) lesions that were unsuitable for OCT (severe tortuous lesions and ostial lesions). All patients received dual antiplatelet therapy with aspirin (100 mg/day) and clopidogrel (75 mg/day) for at least 8 months after stent implantation. The study subjects were recruited from among patients who had provided written informed consent to OCT-guided PCI and a follow-up OCT examination. The study was approved by the Ethics Committee of Kobe University.

OCT examination

The OCT examination was performed serially, immediately following PCI and at 8-month follow-up after stent implantation. We used an FD-OCT system (C7-XR, St. Jude Medical, St. Paul, MN, USA) in conjunction with a 2.7 F imaging catheter (C7 Dragonfly, LightLab Imaging, Westford, MA, USA). To obtain OCT images, FD-OCT pullbacks were performed at 20 mm/s with a non-occlusive flushing technique using non-ionic contrast media [7]. All images were analyzed by two independent observers, who were blinded to the clinical presentations and lesion characteristics. Cross-sectional OCT images were analyzed frame by frame. Bifurcation lesions with major side branches were excluded from the analysis. To ensure a consistent analysis of segments at baseline and at follow-up OCT, we displayed the baseline and follow-up OCT images side by side and performed serial OCT analysis, using information about the motorized pullback speed, and landmarks such as the presence of calcium deposits, side branches, and plaque shape [4].

Immediately after PCI, we evaluated the presence of acute strut malapposition, the S–V distance and the length of the malapposition, and the characteristics of the underlying plaque. S–V distance was defined as the distance between the center reflection of the strut and the vessel wall. Acute strut malapposition was defined as an S–V distance $>$108 μm; this criterion was determined by adding the actual strut thickness and polymer thickness to the OCT resolution limit ($81 + 7 + 20 = 108$ μm) [8, 9]. Malapposition length was defined as the number of consecutive cross-sections with malapposed struts [4]. It was not possible to avoid acute strut malapposition entirely at the end of the initial procedure, despite all our best efforts to optimize stent apposition by performing balloon post-dilatation, because some target vessels had positive remodeling or had irregular shapes with a variable diameter. Plaque types underneath acute strut malapposition were classified as lipid, calcified, or fibrous (Fig. 1). Lipid plaque was defined as a signal-poor region with diffuse borders, calcified plaque as a well-delineated, signal-poor region with sharp borders, and fibrous plaque as a homogeneous signal-rich region [10]. The plaque type was determined by two independent observers, or after intensive discussion between multiple observers in our institution in the case of disagreement.

At 8 months, we assessed the following: (1) the incidence of resolved, persistent, and late-acquired strut malapposition, (2) the malapposition length of persistent strut malapposition, and (3) the incidence of intra-stent thrombi by OCT. The follow-up OCT assessment was used to classify the strut malapposition as resolved or persistent. Resolved strut malapposition was defined as acute malapposition integrated into the vessel wall, whereas persistent strut malapposition was defined as acute malapposition persisting as incomplete apposition. Late-acquired strut malapposition was defined as malapposition that was not present immediately after the procedure but was observed at follow-up [11]. Intra-stent thrombus was defined as a mass protruding beyond the stent strut into the lumen, with significant attenuation behind the mass (Fig. 2) [12]. In addition, we carried out a sub-analysis of the same items according to the location of the acute strut malapposition (stent edge or stent body). The stent edge was defined as the proximal or distal stent segment, within 5 mm of the end of the stent.

Statistical analysis

Qualitative data are presented as frequencies and quantitative data as mean values ± SD. Categorical data were

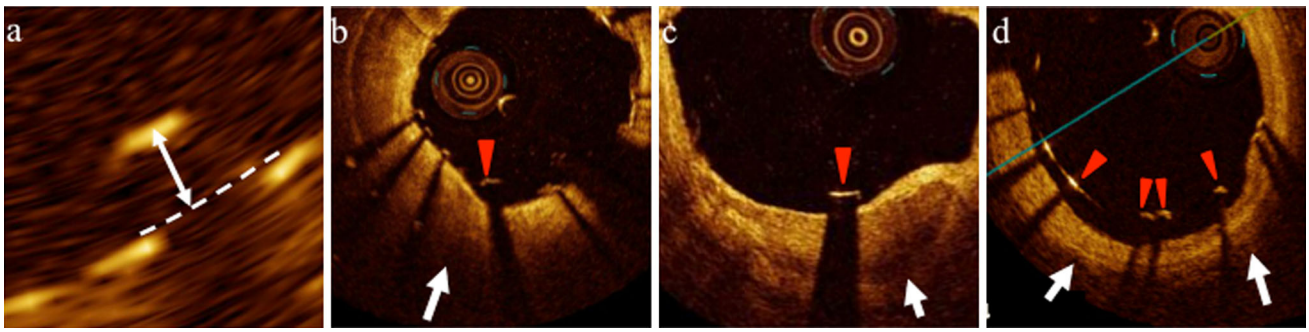

Fig. 1 Representative examples of optical coherence tomography images. **a** Measurement of strut–vessel (S–V) distance; **b** acutely malapposed strut over lipid plaque; **c** acutely malapposed strut over calcified plaque; **d** acutely malapposed strut over fibrous plaque. *Red arrowheads* indicate acutely malapposed struts. *White arrowheads* indicate the corresponding plaque type underneath acutely malapposed strut

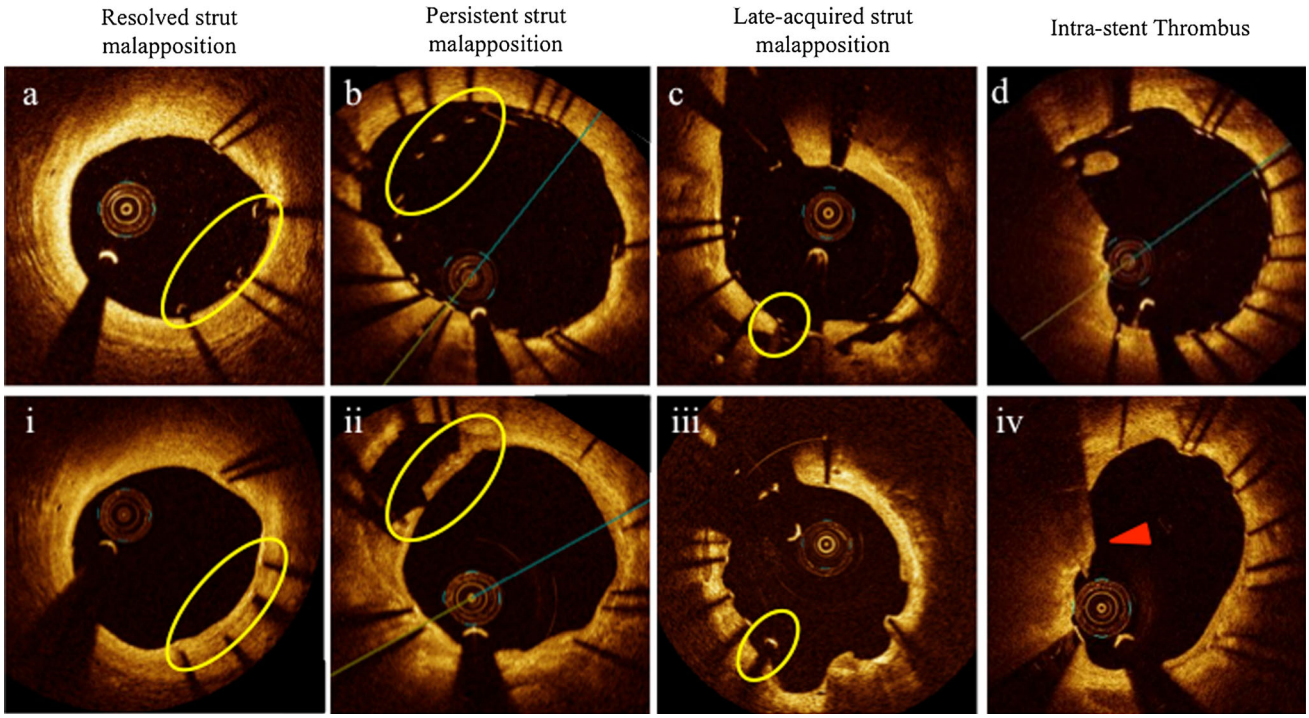

Fig. 2 Representative optical coherence tomography (OCT) images of the time course of acute strut malapposition and intra-stent thrombus. From **a** to **d** baseline OCT images immediately after PCI; from **i** to **iv** corresponding OCT images at 8-month follow-up; **i** resolved strut malapposition; **ii** persistent strut malapposition; **iii** late-acquired strut malapposition; **iv** intra-stent thrombus at 8-month follow-up. *Red arrowhead* indicates intra-stent thrombus

compared using either the Chi square test or Fisher's exact test. Continuous variables were compared using an unpaired or paired Student's *t* test or the Mann–Whitney U test. We performed a receiver operating characteristics (ROC) analysis of the S–V distance to identify the optimal cutoff value for predicting the natural course of acute strut malapposition during the follow-up (resolved or persistent). Other quantitative data were analyzed using an unpaired *t*-test. A two-sided *P* value <0.05 was considered statistically significant. Statistical analyses were performed using MedCalc version 12.4.0 (MedCalc Software, Mariakerke, Belgium).

Results

We consecutively enrolled 236 patients with de novo native coronary lesions who were treated with 321 EES between July 2010 and November 2011. Among these, 65 patients underwent FD-OCT (C7-OCT)-guided PCI. At

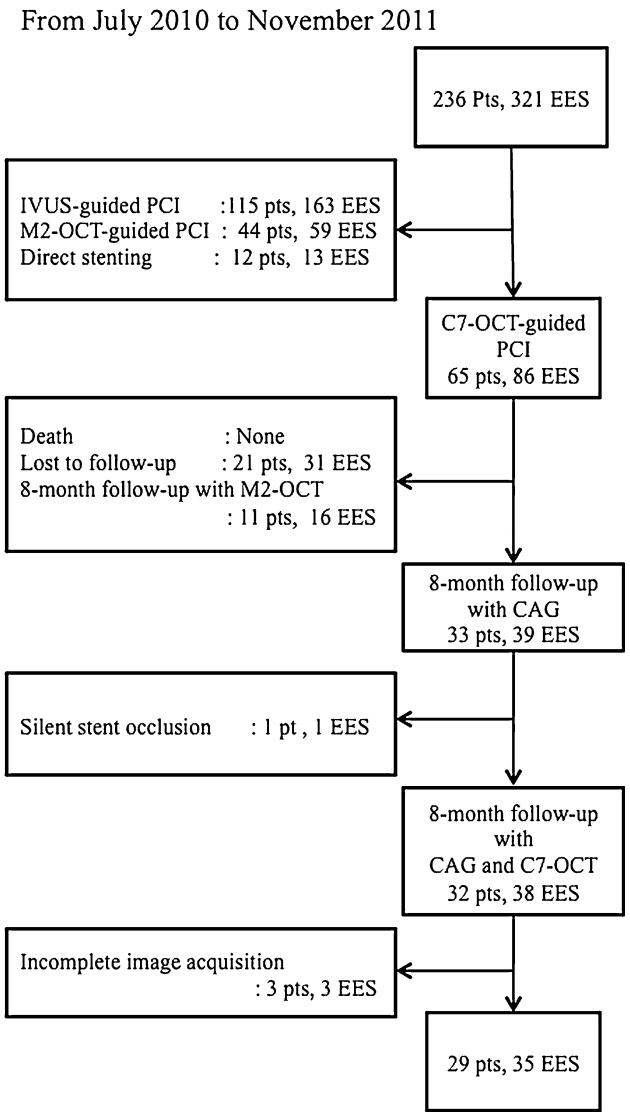

Fig. 3 Cohort of this study. *IVUS* intravascular ultrasound, *PCI* percutaneous coronary intervention, *C7-OCT* C7-XR optical coherence tomography intravascular imaging system, *M2-OCT* M2 optical coherence tomography intravascular imaging system, *EES* everolimus-eluting stents, *CAG* coronary angiography

8 months after EES implantation, 21 patients were lost to follow-up, 11 had a follow-up FD-OCT performed with a different FD-OCT system (M2-OCT), and one suffered from silent stent occlusion, where it was not possible to perform a follow-up FD-OCT examination. As a result, 32 patients with 38 EES underwent FD-OCT monitoring at the index PCI as well as follow-up FD-OCT performed with the same system (C7-OCT) 8 months post-implantation. Three patients with 3 EES were excluded because of incomplete image acquisition. Thus, we investigated a total of 29 patients (25 males; age 66 ± 9.5 years) with 35 EES (Fig. 3). Baseline patient demographic, lesion, procedural, and laboratory data are shown in Table 1. In all stents,

Table 1 Patient Characteristics

Number of patients	29
Number of EES	35
Male	25 (86)
Age (years)	66 ± 9.5
Follow-up (days)	254 ± 49
Diabetes mellitus	15 (52)
Hypertension	20 (69)
Dyslipidemia	25 (86)
History of smoking	19 (65)
Previous MI	7 (24)
Stable angina	26 (90)
Unstable angina	3 (10)
LAD/LCx/RCA/LMT	17 (48)/3 (9)/14 (40)/1 (3)
Type B2/C lesions[a]	21 (72)
CTO	3 (10)
Stent diameter (mm)	3.0 ± 0.3
Stent length (mm)	18.7 ± 5.6
Stent implantation pressure (atm)	10.3 ± 1.6
Post dilatation	21 (60)
Largest balloon size for dilatation (mm)	3.1 ± 0.4
Maximum inflation pressure (atm)	13.7 ± 3.8
Laboratory data	
Fasting blood glucose (mg/dL)	109 ± 30
LDL-cholesterol (mg/dL)	88 ± 30
HDL-cholesterol (mg/dL)	49 ± 17
Triglycerides (mg/dL)	136 ± 57
HbA1c (%)	6.4 ± 1.2

Data are presented as mean ± SD or number (%)

EES everolimus-eluting stent(s), *MI* myocardial infarction, *LAD* left anterior descending artery, *LCx* left circumflex artery, *RCA* right coronary artery, *LMT* left main trunk, *CTO* chronic total occlusion, *LDL* low-density lipoprotein, *HDL* high-density lipoprotein, *HbA1c* hemoglobin A1c

[a] Based on American College of Cardiology/American Heart Association classification

angiographic optimization was accomplished after PCI. The mean interval before follow-up angiography was 254 ± 49 days. During the follow-up, major adverse cardiac events (MACE; defined as cardiac death, nonfatal myocardial infarction, or target lesion revascularization) occurred in one patient, who suffered from ischemia-driven target lesion revascularization due to in-stent restenosis. There was no patient with stent thrombosis.

Incidence of persistent, resolved, and late-acquired strut malapposition

Strut malapposition was observed in 62.9 % of enrolled stents (22/35 stents) immediately after stenting (acute strut malapposition), and in 31.4 % (11/35 stents) at follow-up.

Among the total of 22 EES with acute strut malapposition, serial OCT analysis revealed that 11 stents (11/22, 50.0 %) were partially resolved, with at least one persistent strut malapposition at follow-up, while 11 stents (11/22, 50.0 %) were completely resolved, with no strut malapposition observed on the follow-up OCT images. Late-acquired strut malapposition was observed in 4 stents (4/35, 11.4 %), in all of which acute strut malapposition had been observed at a different site. One late-acquired strut malapposition occurred in an EES that was well-apposed on intima, but with dissection of the media. The other three late-acquired strut malapposition cases involved struts with thrombus attachment. In contrast, no late-acquired strut malapposition was seen in stents that had no acute strut malapposition.

According to a strut-based analysis, 569 struts among a total of 29,168 struts (2.04 %) showed acute strut malapposition on post-procedural OCT images. Among these, serial OCT analysis revealed persistent strut malapposition of 139 struts (24.4 %), but the other 430 struts (75.6 %) had resolved by the time of follow-up (resolved strut malapposition), while there were 29 struts with newly appearing late-acquired strut malapposition.

The incidence of intra-stent thrombi on the follow-up OCT images was higher in stents with at least one persistent strut malapposition than in those with none [4/11 (36.3 %), vs. 0/24 (0 %), respectively; $P = 0.006$].

Relation between S–V distance and natural course of acute strut malapposition

The mean S–V distance for all acute strut malapposition on post-procedural OCT images was 321 ± 230 μm. The mean S–V distance of persistent strut malapposition was significantly greater than that of resolved strut malapposition (600 ± 294 vs. 231 ± 95 μm; $P < 0.0001$). Based on ROC analysis, the best cutoff value of S–V distance for predicting resolved strut malapposition was ≤380 μm, with a maximum sensitivity of 93.5 % and a specificity of 69.8 % (area under the curve, AUC = 0.878) (Fig. 4).

According to a cross-sectional analysis, the average malapposition length immediately post-PCI also decreased significantly by 8-month follow-up (number of cross sections with malapposition; from 12 ± 10 to 3 ± 5; $P < 0.0001$).

Relation between underlying plaque type and natural course of acute strut malapposition

Among 22 EES with acute strut malapposition, most of the stented lesions were associated with lipid or fibrous plaque [lipid: 14/22 stents (63.6 %), calcified: 3/22 (13.6 %), and fibrous: 15/22 (68.1 %)]. In the 569 cases of acute strut malapposition, lipid plaque was predominantly observed [lipid: 340 (59.8 %), calcified: 22 (3.9 %), and fibrous: 207 (36.3 %)], but the average number of malapposed struts in relation to the number of stents over each kind of plaque was similar for all kinds of plaque (lipid: 22.7 ± 29.9 struts, calcified: 7.3 ± 4.5, and fibrous: 14.8 ± 15.7; P = NS).

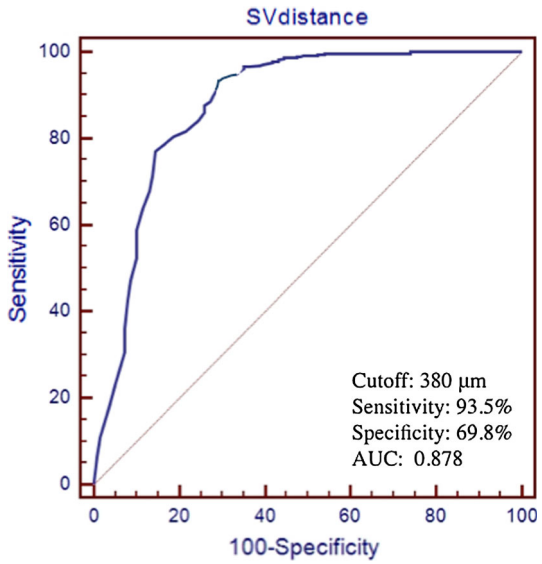

Fig. 4 Receiver operating characteristics analysis of strut–vessel (S–V) distance. The best cutoff value of S–V distance for predicting resolved strut malapposition was 380 μm [sensitivity: 93.5 %, specificity: 69.8 %, area under the curve (AUC): 0.878, 95 % confidence interval (CI) 0.848–0.904]

In the 123 cases of acute strut malapposition with an S–V distance >380 μm, lipid plaque was most common and no cases of calcified plaque were observed [lipid 108 (87.8 %), calcified 0 (0 %), and fibrous 15 (12.2 %)]. Acute strut malapposition with an S–V distance >380 μm tended to remain as persistent strut malapposition, regardless of the plaque type [lipid: 108 acute malapposed struts → 83 persistent malapposed struts (76.9 %); fibrous: 15 → 13 (86.7 %); $P = 0.52$].

In contrast, in the 446 cases of acute strut malapposition with an S–V distance ≤380 μm, the plaque underneath malapposed strut was classified as follows: lipid 232 (52.0 %), calcified 22 (4.9 %), and fibrous 192 (43.0 %). Strut malapposition with an S–V distance ≤380 μm remained as persistent strut malapposition more frequently over lipid or calcified plaque than over fibrous plaque [lipid: 232 acute malapposed struts → 31 persistent malapposed struts (13.4 %), calcified: 22 → 4 (18.2 %), fibrous: 192 → 8 (4.2 %); $P = 0.001$ for lipid vs. fibrous and $P = 0.02$ for calcified vs. fibrous, respectively] (Fig. 5).

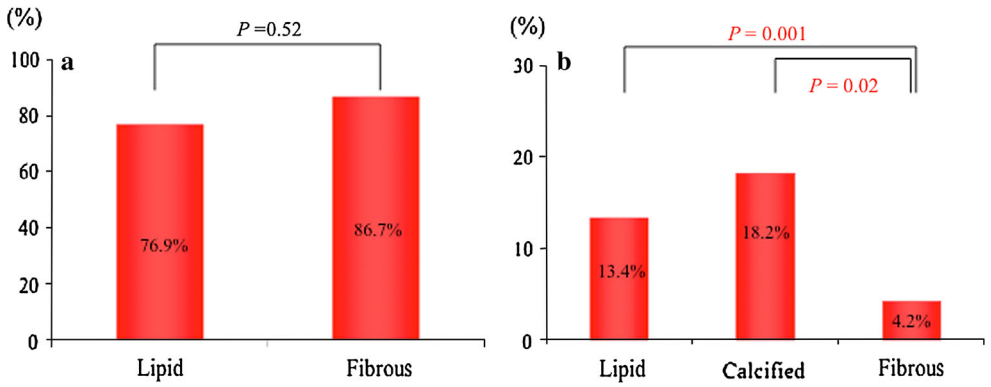

Fig. 5 The incidence of persistent strut malapposition according to the type of underlying plaque. **a** Acute strut malapposition with strut–vessel (S–V) distance >380 μm; **b** acute strut malapposition with S–V distance ≤380 μm

Longitudinal analysis also revealed that acute strut malapposition over lipid plaque persisted more frequently than over fibrous plaque [number of cross sections with malapposition; lipid: 148 → 57 (38.5 %), calcified: 10 → 3 (30 %), fibrous: 90 → 9 (10.0 %); $P < 0.0001$ for lipid vs. fibrous, and $P = 0.36$ for calcified vs. fibrous].

Sub-analysis according to the location of acute strut malapposition

According to the location of acute strut malapposition, 297 (52.2 %) among 569 acutely malapposed struts were located at the stent edge, while the other 272 (47.8 %) were in the stent body. At the stent edge, follow-up OCT showed 47 (15.8 %) persistent malapposed struts and 250 (84.2 %) resolved malapposed struts. In the stent body, 92 (33.8 %) acutely malapposed struts persisted and 180 (66.1 %) had resolved by 8-month follow-up ($P < 0.0001$). As for newly appearing late-acquired strut malapposition, in 11 of 29 struts the malapposition was at the stent edge. The total malapposition length also decreased more at the stent edge than in the stent body [number of cross sections with malapposition; 117 → 23 (19.7 %) vs. 134 → 46 (34.3 %); $P = 0.014$]. The mean S–V distances of both acute strut malapposition and persistent strut malapposition at the stent edge were shorter than those in the stent body (acute strut malapposition: 258 ± 148 vs. 390 ± 279 μm; $P < 0.0001$, and persistent strut malapposition: 453 ± 227 vs. 676 ± 297 μm; $P < 0.0001$). Based on ROC analysis, the best cutoff value of S–V distance for predicting resolved strut malapposition at the stent edge was ≤270 μm, with a maximum sensitivity of 84.0 % and a specificity of 80.9 % (AUC = 0.828), whereas the best cutoff value for the stent body was ≤460 μm, with a maximum sensitivity of 96.1 % and a specificity of 75.0 % (AUC = 0.898) (Fig. 6).

Discussion

The primary findings of this study are as follows. First, at 8-month follow-up, 50 % of EES with acute strut malapposition were completely resolved, with no residual strut malapposition, and approximately 75 % of EES struts with acute strut malapposition were completely resolved. Second, an S–V distance ≤380 μm was the best cutoff value for predicting resolved strut malapposition after EES implantation, with a maximum sensitivity of 93.5 % and a specificity of 69.8 %. Third, acute strut malapposition with a short S–V distance (≤380 μm) remained as persistent strut malapposition more frequently over lipid or calcified plaque than over fibrous plaque, whereas acute strut malapposition with a long S–V distance (>380 μm) tended to remain as persistent strut malapposition, regardless of the plaque type. Lastly, the frequency of intra-stent thrombi was higher in stents with ≥1 persistent strut malapposition on the follow-up OCT images than in those without any strut malapposition.

The incidence of persistent or late-acquired strut malapposition

In this study, acute strut malapposition was observed in 62.9 % of the EES (22/35 stents), among which 11 were partially resolved, with at least one persistent strut malapposition at 8-month follow-up. Late-acquired strut malapposition was observed in 11.4 % of EES. This incidence of late-acquired strut malapposition is higher than in previous IVUS reports, probably because OCT, with its higher resolution, can detect late-acquired strut malapposition more frequently than IVUS [13–15]. This study also demonstrated the following mechanisms of late-acquired strut malapposition: (1) attachment of thrombi to struts post-implant resolved at follow-up; and (2) intima with

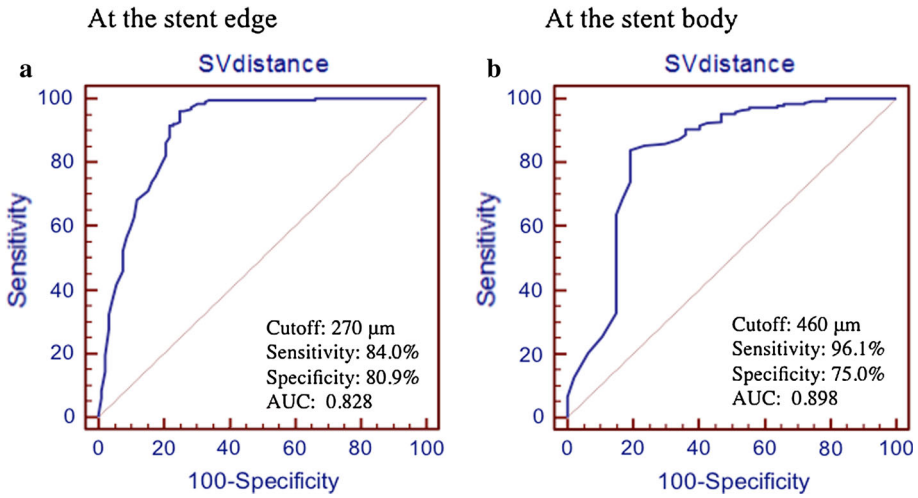

Fig. 6 Receiver operating characteristics analysis of strut–vessel (S–V) distance according to the location of acute strut malapposition. **a** Acute strut malapposition with strut–vessel (S–V) distance at the stent edge; **b** acute strut malapposition with S–V distance in the stent body At the stent edge, the best cutoff value of S–V distance for predicting resolved strut malapposition was ≤270 µm [sensitivity: 84.0 %, specificity; 80.9 %, area under the curve (AUC) = 0.828, 95 % confidence interval (CI) 0.789–0.883]. The best cutoff value for the stent body was ≤460 µm (sensitivity: 96.1 %, specificity; 75.0 %, AUC = 0.898, 95 % CI 0.922–0.984)

dissection of the media immediately after PCI was attached to the media at follow-up.

Relation between S–V distance and natural course of acute strut malapposition

An S–V distance ≤380 µm was the best cutoff value for predicting resolved strut malapposition after EES implantation, with a maximum sensitivity of 93.5 % and a specificity of 69.8 %. We previously conducted an OCT study in first-generation DES using serial OCT observations similar to those in the present study [4]. According to that study, the cutoff value of S–V distance for predicting resolved strut malapposition after first-generation DES implantation was ≤260 µm [4]. This indicates that the cutoff value for EES is longer than for first-generation DES, even though there were no differences between the two studies in baseline patient, lesion, or procedural characteristics, and laboratory data, except for the FD-OCT systems used (M2-OCT and C7-OCT). One explanation for this phenomenon could be that EES have thinner struts, a lower drug load, and a more biocompatible polymer compared to first-generation DES, so that the arterial healing reaction is promoted in the case of EES [8].

Relation between underlying plaque type and natural course of acute strut malapposition

Acute strut malapposition with an S–V distance shorter than the cutoff value (≤380 µm) remained as persistent strut malapposition more frequently over lipid or calcified plaque than over fibrous plaque. Various factors, such as patient and lesion characteristics, procedural factors, type of stents, and S–V distance, may have an impact on the healing process of acute strut malapposition following first-generation DES implantation [4, 6, 15–17]. In the 2nd generation DES era, Gutiérrez-Chico et al. [5] reported that the S–V distance of acute strut malapposition was the best predictive factor for persistent incomplete apposition . To the best of our knowledge, this is the first report to assess the impact of the plaque type underneath acutely malapposed struts, as well as S–V distance, on the course of acute strut malapposition after EES implantation.

Both everolimus and sirolimus, which are highly lipophilic agents [18], have a high affinity for lipid-rich plaque and remain there for longer periods. Lipid plaque is more avascular compared with regions of fibrous dominant plaque, and has fewer cells, resulting in less coverage by migrating and proliferating cells from adjacent areas [15]. As for calcified plaque, Kimura et al. [19] indicated that superficial calcification impeded resolution of a malapposed strut by inhibiting persistent neointimal hyperplasia . Therefore, lipid and calcified plaque may influence neointimal growth.

The findings of our study imply that when acute strut malapposition is observed over lipid or calcified plaque, even if the S–V distance is less than the cutoff value of 380 µm, it is better to optimize stent apposition with OCT guidance at the index PCI.

Relation between incidence of persistent or late-acquired strut malapposition and frequency of intra-stent thrombi

The frequency of intra-stent thrombi in stents with strut malapposition at follow-up OCT was significantly higher

than in those without any strut malapposition [with strut malapposition: 4/11 (36.3 %) vs. without: 0/24 (0 %), $P = 0.006$]. According to a previous OCT study reported by Kawamori et al. [4] intra-stent thrombi within first-generation DES were observed regardless of the presence of strut malapposition at follow-up [with strut malapposition: 44.4 % (4/9 stents) vs. without: 12.9 % (4/31 stents), $P = 0.20$]. We speculated that this discrepancy between EES and first-generation DES could be attributed to several factors, as follows. First, strut condition (e.g., extent of neointimal coverage or incidence of malapposed struts) after EES implantation at mid-term follow-up was improved compared to first-generation DES, because of the improved design of strut, drug load and polymer, as previously reported [8]. Second, it is possible that endothelial function after EES implantation may be better than that after first-generation DES, resulting in its lower thrombogenicity. A recent clinical study suggested that coronary artery endothelial dysfunction with impaired vasomotor function was associated with the presence of thrombi or incompletely neointimal coverage (grade 0/1 accessed by angioscopy) after first-generation DES implantation [20].

Sub-analysis according to the location of acute strut malapposition

A sub-analysis based on the location of the acute strut malapposition demonstrated that (1) acutely malapposed struts at the stent edge were more likely to be resolved than those in the stent body, because of their shorter S–V distance, and (2) the best cutoff value of S–V distance at the stent edge for predicting resolved strut malapposition was $\leq$270 μm. It is still unknown whether there are differences between the mechanisms of arterial healing at the edge and in the body of 2nd generation DES. It was recently suggested that the spreading of smooth muscle cells from adjacent vessel wall over the surface of the malapposed struts, covering the detached malapposed strut, could play a possible role in arterial healing after DES implantation [5]. The distribution of wall shear stress, or the impact of the underlying tissue character on the strut coverage process could be different between the stent edge and body. Further large-scale studies are warranted to elucidate the post-stent healing response in more detail.

Limitations

Our study has a number of limitations. First, it was a retrospective study based on a relatively limited sample size, raising the possibility of selection bias. Second, although we carefully reviewed both post-stenting and follow-up OCT images, it is sometimes difficult to completely match the lesions on the two sets of images. Third, although OCT is a high-resolution modality, it may not be able to differentiate neointima from organized white thrombus, as both show high backscatter on the image. A smooth-shaped thrombus might thus be misdiagnosed as neointima. Fourth, the cutoff value obtained by ROC analysis depends on the study design, including the stent structure, loaded drug, strut thickness, and the patients' background; here, we assessed EES in patients who did not have acute coronary syndromes. Finally, the strut-based analysis was performed for every frame interval. The stent-based analysis in our methodology equally evaluated stents with a single-malapposed strut as well as stents with large sections of malapposed struts. As this methodology is different from that of previous IVUS studies, the results of the present study might not be directly comparable.

Clinical implications

According to our findings, in the 2nd generation DES era, the presence of strut malapposition in the chronic phase could be the substrate for stent thrombosis after EES implantation, and strut malapposition might be more prone to persist over lipid or calcified plaque. Therefore, balloon post-dilation should be performed, especially if the S–V distance is greater than 380 μm, the plaque is lipid-rich or calcified, or the location of the strut malapposition is at the stent edge.

Conclusion

Lipid or calcified plaques, together with S–V distance, have an impact on the persistence of strut malapposition after EES implantation, which could be a substrate for intra-stent thrombus attachment and subsequent stent thrombosis. OCT assessment of strut apposition and plaque type underneath EES immediately after PCI may help to optimize stent deployment. Further study is warranted to define an OCT-derived optimal endpoint for stent placement in various types of lesion.

Conflict of interest No conflicts of interest.

References

1. Gonzalo N, Serruys PW, Okamura T, Shen ZJ, Onuma Y, Garcia-Garcia HM, Sarno G, Schultz C, van Geuns RJ, Ligthart J, Regar E (2009) Optical coherence tomography assessment of the acute effects of stent implantation on the vessel wall: a systematic quantitative approach. Heart 95(23):1913–1919. doi:10.1136/hrt.2009.172072

2. Kawamori H, Shite J, Shinke T, Otake H, Sawada T, Kato H, Miyoshi N, Yoshino N, Kozuki A, Hariki H, Inoue T, Hirata K (2010) The ability of optical coherence tomography to monitor percutaneous coronary intervention: detailed comparison with intravascular ultrasound. J Invasive Cardiol 22(11):541–545
3. Kume T, Okura H, Miyamoto Y, Yamada R, Saito K, Tamada T, Koyama T, Neishi Y, Hayashida A, Kawamoto T, Yoshida K (2012) Natural history of stent edge dissection, tissue protrusion and incomplete stent apposition detectable only on optical coherence tomography after stent implantation–preliminary observation. Circ J 76(3):698–703
4. Kawamori H, Shite J, Shinke T, Otake H, Matsumoto D, Nakagawa M, Nagoshi R, Kozuki A, Hariki H, Inoue T, Osue T, Taniguchi Y, Nishio R, Hiranuma N, Hirata KI (2013) Natural consequence of post-intervention stent malapposition, thrombus, tissue prolapse, and dissection assessed by optical coherence tomography at mid-term follow-up. Eur Heart J Cardiovasc Imaging. doi:10.1093/ehjci/jes299
5. Gutierrez-Chico JL, Wykrzykowska J, Nuesch E, van Geuns RJ, Koch KT, Koolen JJ, di Mario C, Windecker S, van Es GA, Gobbens P, Juni P, Regar E, Serruys PW (2012) Vascular tissue reaction to acute malapposition in human coronary arteries: sequential assessment with optical coherence tomography. Circ Cardiovasc Interv 5(1):20–29, S21–28. doi:10.1161/CIRCINTERVENTIONS.111.965301
6. Gonzalo N, Barlis P, Serruys PW, Garcia-Garcia HM, Onuma Y, Ligthart J, Regar E (2009) Incomplete stent apposition and delayed tissue coverage are more frequent in drug-eluting stents implanted during primary percutaneous coronary intervention for ST-segment elevation myocardial infarction than in drug-eluting stents implanted for stable/unstable angina: insights from optical coherence tomography. JACC Cardiovasc Interv 2(5):445–452. doi:10.1016/j.jcin.2009.01.012
7. Tu S, Holm NR, Koning G, Huang Z, Reiber JH (2011) Fusion of 3D QCA and IVUS/OCT. Int J Cardiovasc Imaging 27(2):197–207. doi:10.1007/s10554-011-9809-2
8. Inoue T, Shite J, Yoon J, Shinke T, Otake H, Sawada T, Kawamori H, Katoh H, Miyoshi N, Yoshino N, Kozuki A, Hariki H, Hirata K (2011) Optical coherence evaluation of everolimus-eluting stents 8 months after implantation. Heart 97(17):1379–1384. doi:10.1136/hrt.2010.204339
9. Tanigawa J, Barlis P, Di Mario C (2007) Intravascular optical coherence tomography: optimisation of image acquisition and quantitative assessment of stent strut apposition. EuroIntervention 3(1):128–136
10. Yabushita H, Bouma BE, Houser SL, Aretz HT, Jang IK, Schlendorf KH, Kauffman CR, Shishkov M, Kang DH, Halpern EF, Tearney GJ (2002) Characterization of human atherosclerosis by optical coherence tomography. Circulation 106(13):1640–1645
11. Guo N, Maehara A, Mintz GS, He Y, Xu K, Wu X, Lansky AJ, Witzenbichler B, Guagliumi G, Brodie B, Kellett MA Jr, Dressler O, Parise H, Mehran R, Stone GW (2010) Incidence, mechanisms, predictors, and clinical impact of acute and late stent malapposition after primary intervention in patients with acute myocardial infarction: an intravascular ultrasound substudy of the harmonizing outcomes with revascularization and stents in acute myocardial infarction (HORIZONS-AMI) trial. Circulation 122(11):1077–1084. doi:10.1161/CIRCULATIONAHA.109.906040
12. Jang IK, Tearney GJ, MacNeill B, Takano M, Moselewski F, Iftima N, Shishkov M, Houser S, Aretz HT, Halpern EF, Bouma BE (2005) In vivo characterization of coronary atherosclerotic plaque by use of optical coherence tomography. Circulation 111(12):1551–1555. doi:10.1161/01.CIR.0000159354.43778.69
13. Shimohama T, Ako J, Yamasaki M, Otake H, Tsujino I, Hasegawa T, Nakatani D, Sakurai R, Chang H, Kusano H, Waseda K, Honda Y, Stone GW, Saito S, Fitzgerald PJ, Sudhir K (2010) SPIRIT III JAPAN versus SPIRIT III USA: a comparative intravascular ultrasound analysis of the everolimus-eluting stent. Am J Cardiol 106(1):13–17. doi:10.1016/j.amjcard.2010.02.008
14. Ozaki Y, Okumura M, Ismail TF, Naruse H, Hattori K, Kan S, Ishikawa M, Kawai T, Takagi Y, Ishii J, Prati F, Serruys PW (2010) The fate of incomplete stent apposition with drug-eluting stents: an optical coherence tomography-based natural history study. Eur Heart J 31(12):1470–1476. doi:10.1093/eurheartj/ehq066
15. Jang IK, Bouma BE, Kang DH, Park SJ, Park SW, Seung KB, Choi KB, Shishkov M, Schlendorf K, Pomerantsev E, Houser SL, Aretz HT, Tearney GJ (2002) Visualization of coronary atherosclerotic plaques in patients using optical coherence tomography: comparison with intravascular ultrasound. J Am Coll Cardiol 39(4):604–609
16. Nakazawa G, Finn AV, Joner M, Ladich E, Kutys R, Mont EK, Gold HK, Burke AP, Kolodgie FD, Virmani R (2008) Delayed arterial healing and increased late stent thrombosis at culprit sites after drug-eluting stent placement for acute myocardial infarction patients: an autopsy study. Circulation 118(11):1138–1145. doi:10.1161/CIRCULATIONAHA.107.762047
17. Kubo T, Imanishi T, Kitabata H, Kuroi A, Ueno S, Yamano T, Tanimoto T, Matsuo Y, Masho T, Takarada S, Tanaka A, Nakamura N, Mizukoshi M, Tomobuchi Y, Akasaka T (2008) Comparison of vascular response after sirolimus-eluting stent implantation between patients with unstable and stable angina pectoris: a serial optical coherence tomography study. JACC Cardiovasc Imaging 1(4):475–484. doi:10.1016/j.jcmg.2008.03.012
18. Otake H, Shite J, Ako J, Shinke T, Tanino Y, Ogasawara D, Sawada T, Miyoshi N, Kato H, Koo BK, Honda Y, Fitzgerald PJ, Hirata K (2009) Local determinants of thrombus formation following sirolimus-eluting stent implantation assessed by optical coherence tomography. JACC Cardiovasc Interv 2(5):459–466. doi:10.1016/j.jcin.2009.03.003
19. Levin AD, Vukmirovic N, Hwang CW, Edelman ER (2004) Specific binding to intracellular proteins determines arterial transport properties for rapamycin and paclitaxel. Proc Natl Acad Sci U S A 101(25):9463–9467. doi:10.1073/pnas.0400918101
20. Kimura M, Mintz GS, Carlier S, Takebayashi H, Fujii K, Sano K, Yasuda T, Costa RA, Costa JR Jr, Quen J, Tanaka K, Lui J, Weisz G, Moussa I, Dangas G, Mehran R, Lansky AJ, Kreps EM, Collins M, Stone GW, Moses JW, Leon MB (2006) Outcome after acute incomplete sirolimus-eluting stent apposition as assessed by serial intravascular ultrasound. Am J Cardiol 98(4):436–442. doi:10.1016/j.amjcard.2006.02.050